Critical slowing down and dispersion of avalanche upconversion dynamics

Q. Shu and S. C. Rand
Division of Applied Physics, 1049 Randall Laboratory, University of Michigan, Ann Arbor, Michigan 48109-1120
(Received 23 September 1996)

The temporal response time on an avalanche upconversion transition is shown to undergo critical slowing down near the avalanche threshold. Also, the nonlinear refractive index is predominantly real, despite the resonant nature of the avalanche phenomenon. These findings are in excellent agreement with density-matrix analyses showing that cross relaxation dramatically alters the effective excited-state lifetime and that off-resonance absorption curiously dominates the wavelength dependence of the nonlinear refractive index. [S0163-1829(97)04214-8]

I. INTRODUCTION

Since its discovery,[1] avalanche upconversion has been of interest for solid-state lasers[2] because of the strong absorption it generates in spectral regions normally devoid of ground-state optical transitions in concentrated rare-earth and transition-metal crystals. Materials displaying the avalanche phenomenon universally exhibit cross-relaxation dynamics in connection with an excited-state optical resonance. By tuning light into coincidence with an excited-state absorption resonance and providing sufficient power density to exceed the avalanche threshold, intense luminescence can be generated at wavelengths shorter than the incident one.

Most earlier investigations focused on population inversion conditions in avalanche systems. Only a few studies have examined the nonlinear response[3,4] associated with avalanche dynamics. In an earlier publication,[5] we reported measurements of nonlinear refractive indices as a function of incident intensity, using a two-beam coupling approach. Here we describe experimental observations of a previously unreported characteristic[6] of avalanche nonlinearities, namely critical slowing down of the effective response time. We furnish the theoretical basis necessary to understand this result, together with a detailed explanation of the frequency dependence of the nonlinear refractive index. Avalanche upconversion is shown to be an example of surprising, but quite general, dynamics in which the refractive index changes associated with polarization on an excited-state resonance are primarily real, controlled by the off-resonant contributions from weak ground-state absorption.

II. THEORY

A. Steady-state dynamics

To formulate time-dependent analysis of dynamics in an avalanche system, it is first necessary to establish a steady-state description of the occupation of energy levels. To this end we begin by considering the atomistic model of the avalanche process illustrated in Fig. 1. The basic dynamics consist of excitation on an excited-state transition, followed by internal relaxation to a level which participates in cross relaxation with a second atom in its ground state. The Hamiltonian for such a system can be written as $H=H_0+H_{\rm int}$ where H_0 is the unperturbed Hamiltonian and $H_{\rm int}$ describes its interaction with the field ($H_{\text{atom-field}}=-\mu\cdot\mathbf{E}$) and with other atoms ($H_{\text{atom-atom}}$). Treating relaxation processes other than cross relaxation phenomenologically, the equation of motion for the density matrix is

$$i\hbar\dot{\rho}=[H,\rho]+\text{relaxation terms.} \tag{1}$$

Hence equations for the temporal evolution of individual elements of the density matrix are

$$\dot{\rho}_{11}=\gamma_2\rho_{22}+\gamma_{31}\rho_{33}+\gamma_{41}\rho_{44}-\alpha\rho_{11}\rho_{33}+\beta\rho_{22}^2-BI(\rho_{11}-\rho_{33}), \tag{2}$$

$$\dot{\rho}_{22}=-\gamma_2\rho_{22}+\gamma_{32}\rho_{33}+\gamma_{42}\rho_{44}+2\alpha\rho_{11}\rho_{33}-2\beta\rho_{22}^2-iV_{24}\rho_{42}+iV_{42}\rho_{24}, \tag{3}$$

$$\dot{\rho}_{33}=-\gamma_3\rho_{33}+\gamma_{43}\rho_{44}-\alpha\rho_{11}\rho_{33}+\beta\rho_{22}^2+BI(\rho_{11}-\rho_{33}), \tag{4}$$

$$\dot{\rho}_{44}=-\gamma_4\rho_{44}+iV_{42}\rho_{24}-iV_{24}\rho_{42}, \tag{5}$$

$$\dot{\rho}_{24}=(i\omega_{42}-\Gamma_{42})\rho_{24}-iV_{24}(\rho_{44}-\rho_{22}), \tag{6}$$

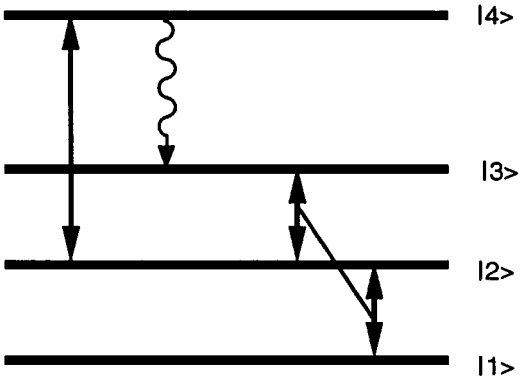

FIG. 1. Schematic illustration of the basic dynamics in the avalanche model. Absorption of light on the transition between states $|2\rangle$ and $|4\rangle$ is followed by internal relaxation to state $|3\rangle$ from which cross relaxation with a ground-state neighbor can occur.

$$\rho_{42}=\rho_{24}^{*}. \tag{7}$$

In these equations, ω_{42} is the optical transition frequency between state $|2\rangle$ and $|4\rangle$, the γ_i is the population decay rate of level i ($i=2,3,4$), Γ_{42} is the dephasing rate of the optical transition (including dephasing caused by energy migration), α is the cross-relaxation coefficient, and β is the coefficient for the reverse reaction. B is the Einstein coefficient of stimulated absorption and emission, and I is the input intensity.

Taking the input field to be of the form $E=\tilde{E}e^{-i\omega t}+\text{c.c.}$, the matrix element of the atom-field interaction in the rotating wave approximation can be written as

$$V_{24}=V_{42}^{*}=\langle 2|H_{\text{atom-field}}|4\rangle=\tfrac{1}{2}\ \Omega_{24}e^{i\omega t}. \tag{8}$$

The quantity $\Omega_{24}=-2\mu_{24}\tilde{E}^{*}/\hbar$ is related to the intensity according to

$$I=\frac{1}{2}\ \varepsilon c|2\tilde{E}|^{2}=\frac{\varepsilon c\hbar^{2}}{2\mu_{24}^{2}}\ |\Omega_{24}|^{2}, \tag{9}$$

where $\mu_{24}=\langle 2|-e\mathbf{r}|4\rangle$ is the transition dipole moment, ε is the dielectric constant of the medium, c is the speed of light in vacuum, and $\hbar$ is Planck's constant.

In a closed system we can easily solve for steady-state behavior. The results are

$$\rho_{44}=f\rho_{22}, \tag{10}$$

$$\rho_{33}=k\rho_{22}+\tfrac{1}{2}\,g, \tag{11}$$

$$\rho_{22}=\frac{-a_1-\sqrt{a_1^{2}-4a_2a_0}}{2a_2}. \tag{12}$$

The ground-state occupation is determined by the closure relation $\rho_{11}+\rho_{22}+\rho_{33}+\rho_{44}=1$. For convenience in simplifying these expressions, several parameters have been introduced:

$$f=\frac{1/2|\Omega_{24}|^{2}\Gamma_{42}/\gamma_4}{\Delta^{2}+\Gamma_{42}^{2}+1/2|\Omega_{24}|^{2}\Gamma_{42}/\gamma_4}, \tag{13}$$

$$g=\frac{4B'|\Omega_{24}|^{2}}{\gamma_3+\gamma_{31}+4B'|\Omega_{24}|^{2}}, \tag{14}$$

$$k=-g\ \frac{1+f}{2}+\frac{(\gamma_{43}-\gamma_{41})f-\gamma_2}{\gamma_3+\gamma_{31}}\ (1-g), \tag{15}$$

$$a_0=g[\,\alpha(1-\tfrac{1}{2}g)+\tfrac{1}{2}\,\gamma_{32}], \tag{16}$$

$$a_1=-\gamma_2-(\gamma_{41}+\gamma_{43})f+[\,\gamma_{32}+2\alpha(1-g)]k-\alpha g(1+f\,), \tag{17}$$

$$a_2=-2\alpha(1+f+k)k-2\beta, \tag{18}$$

The quantity B' in Eq. (14) is a scaled Einstein coefficient given by $B'=BI/|\Omega_{24}|^{2}$.

Notice that the quantity g is related to the off-resonance absorption rate. As g approaches zero, the appearance of avalanche emission above a certain intensity becomes more and more abrupt, although the value of the threshold intensity changes very little. In the limit $g=0$, the occupation of the excited state can be written as

$$\rho_{22}=\frac{-a_1-|a_1|}{2a_2}. \tag{19}$$

Clearly, for $a_1<0$ one obtains $\rho_{22}=0$, whereas for $a_1>0$ one finds the nonzero value $\rho_{22}=-a_1/a_2$, and the excited state becomes occupied. In this limit the boundary of the dynamical phase transition which occurs at avalanche threshold is well defined and given simply by the condition $a_1=0$. The threshold does not depend sensitively on detuning from the ground-state transition under these conditions, but does depend strongly on detuning from the excited-state resonance. When dephasing and detuning are included, the threshold condition for avalanche occurrence can be given in terms of a threshold value for f which is

$$f_{\text{th}}=\frac{\gamma_2(\alpha+\gamma_3)}{(\alpha-\gamma_{31})(\gamma_{43}-\gamma_{41})-(\gamma_3+\gamma_{31})\gamma_{41}}. \tag{20}$$

To complete these results we add the solution for the off-diagonal element ρ_{24}, which is of the form $\rho_{24}=\tilde{\rho}_{24}e^{i\omega t}$, $\tilde{\rho}_{24}$ being its slowly varying amplitude. Writing out this amplitude explicitly in terms of real and imaginary parts according to $\tilde{\rho}_{24}=u+iv$, the expectation value of the atomic polarization can then be determined from the relation

$$p(t)=\text{Tr}(\rho\mu)=\mu_{24}(u-iv)e^{-i\omega t}+\text{c.c.}, \tag{21}$$

for wavelengths in the vicinity of the avalanche transition. The solutions for u and v are given by

$$u=\frac{\Delta\gamma_4}{\Omega_{24}\Gamma_{42}}\ f\rho_{22}, \tag{22}$$

$$v=\frac{\gamma_4}{\Omega_{24}}\ f\rho_{22}. \tag{23}$$

The macroscopic nonlinear polarization density $P(t)=Np(t)$ has a slowly varying amplitude given by $\tilde{P}(\omega)=N\mu_{24}(u-iv)$ from which the effective nonlinear susceptibility can be determined. This is accomplished by first identifying the full nonlinear susceptibility $\chi^{(\text{NL})}$ according to the relation $\tilde{P}^{(\text{NL})}(\omega)=\chi^{(\text{NL})}(\omega)\tilde{E}(\omega)$, and then picking out the effective susceptibility $\chi_{\text{eff}}^{(3)}(\omega)$ using the correspondence $\chi^{(\text{NL})}(\omega)\tilde{E}(\omega)=\chi_{\text{eff}}^{(3)}|\tilde{E}(\omega)|^{2}\tilde{E}(\omega)$. The resulting expression for the effective third-order susceptibility is

$$\chi_{\text{eff}}^{(3)}(\omega)=-N\ \frac{\hbar\gamma_4 f\rho_{22}}{2\Gamma_{24}|\tilde{E}|^{4}}\ (\Delta-i\Gamma_{24}). \tag{24}$$

Notice that the real part of this expression is zero exactly on resonance ($\Delta=0$). This is the usual expectation for optical response in two-level systems.[7]

B. Time-dependent dynamics

For an avalanche system which is not in a steady state, the nonlinear nature of the dynamical equations suggests that numerical techniques must be used to solve for system evo-

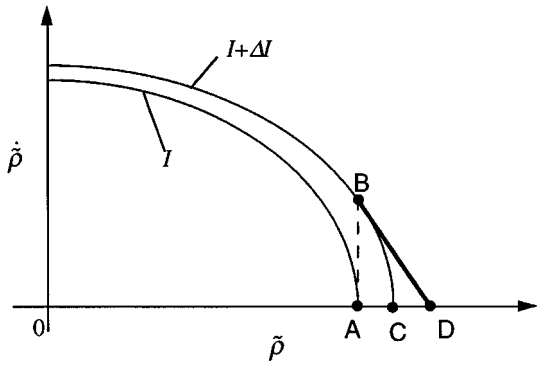

FIG. 2. Phase diagram of temporal evolution in a nonlinear dynamic system, illustrating the idea of linearization of the equation of motion for the density matrix ρ. Initially the system resides in state A, but is perturbed by an intensity change which causes to become nonzero. The system subsequently evolves to state C, for which point D is an adequate approximation for small ΔI.

lution. However when changes are slow or small, an analytic approach is still possible, based on linearization of the dynamical equations.[8]

The basis for the linearization method is illustrated in Fig. 2. This diagram shows a $(\dot{\tilde{\rho}},\tilde{\rho})$ phase space of solutions to the equations of motion of the density matrix for two input intensities I and $I+\Delta$. Initially, the system resides in steady state A. When a small intensity step ΔI is applied to the system at $t=0$, its state is displaced to B and subsequently follows a nonlinear trajectory to reach a new steady state C, as time progresses. If ΔI is small enough, we can approximate this evolution using the tangent at B. Then, the line BD replaces the nonlinear trajectory, permitting us to find a linear approximation for the new steady state of the system. Final results were obtained by successive approximations in the limit of $\Delta I \to 0$.

In the rate equation limit, the earlier dynamical equations become

$$\dot{\rho}_{22} = -\gamma_2\rho_{22} + \gamma_{32}\rho_{33} + \gamma_{42}\rho_{44} + 2\alpha\rho_{11}\rho_{33} - 2\beta\rho_{22}^2 - B_{24}I(\rho_{22}-\rho_{44}), \tag{25}$$

$$\dot{\rho}_{33} = -\gamma_3\rho_{33} + \gamma_{43}\rho_{44} - \alpha\rho_{11}\rho_{33} + \beta\rho_{22}^2 + B_{13}I(\rho_{11}-\rho_{33}), \tag{26}$$

$$\dot{\rho}_{44} = -\gamma_4\rho_{44} + B_{24}I(\rho_{22}-\rho_{44}), \tag{27}$$

B_{24} and B_{13} are the effective pumping rates on transitions $|2\rangle \to |4\rangle$ and $|1\rangle \to |3\rangle$, respectively.

Locally linearized versions of these equations[9] are obtained with the following substitutions:

$$\dot{\rho}_{ii} \to [\dot{\rho}_{ii} + \dot{\rho}_{ii}(0)]/2, \tag{28}$$

$$\rho_{ii}\rho_{jj} \to [\rho_{ii}\rho_{jj}(0) + \rho_{ii}(0)\rho_{jj}]/2, \tag{29}$$

$$\rho_{ii} \to [\rho_{ii} + \rho_{ii}(0)]/2 \tag{30}$$

Indices i,j can both take on the values 2, 3, or 4. After substitution, the equations become

$$\dot{\rho}_{22} = a_{22}\rho_{22} + a_{23}\rho_{33} + a_{24}\rho_{44} + c_2, \tag{31}$$

$$\dot{\rho}_{33} = a_{32}\rho_{22} + a_{33}\rho_{33} + a_{34}\rho_{44} + c_3, \tag{32}$$

$$\dot{\rho}_{44} = a_{42}\rho_{22} + a_{43}\rho_{33} + a_{44}\rho_{44} + c_4. \tag{33}$$

The coefficients are defined as follows:

$$a_{22} = -[\gamma_2 + B_{24}I + 4\beta\rho_{22}(0) + 2\alpha\rho_{33}(0)], \tag{34}$$

$$a_{23} = \gamma_{32} + 2\alpha - 2\alpha\rho_{22}(0) - 4\alpha\rho_{33}(0) - 2\alpha\rho_{44}(0), \tag{35}$$

$$a_{24} = \gamma_{42} + B_{24}I - 2\alpha\rho_{33}(0), \tag{36}$$

$$c_2 = -(\gamma_2 + B_{24}I)\rho_{22}(0) + (\gamma_{32} + 2\alpha)\rho_{33}(0) + (\gamma_{42} + B_{24}I)\rho_{44}(0) - \dot{\rho}_{22}(0), \tag{37}$$

$$a_{32} = -[B_{13}I - 2\beta\rho_{22}(0) - \alpha\rho_{33}(0)], \tag{38}$$

$$a_{33} = -[\gamma_3 + 2B_{13}I + \alpha - \alpha\rho_{22}(0) - 2\alpha\rho_{33}(0) - \alpha\rho_{44}(0)], \tag{39}$$

$$a_{34} = \gamma_{43} - B_{13}I + \alpha\rho_{33}(0), \tag{40}$$

$$c_3 = 2B_{13}I - B_{13}I\rho_{22}(0) - (\gamma_3 + 2B_{13}I + \alpha)\rho_{33}(0) + (\gamma_{43} - B_{13}I)\rho_{44}(0) - \dot{\rho}_{33}(0), \tag{41}$$

$$a_{42} = B_{24}I, \tag{42}$$

$$a_{43} = 0, \tag{43}$$

$$a_{44} = -\gamma_4 - B_{24}I, \tag{44}$$

$$c_4 = B_{24}I\rho_{22}(0) - (\gamma_4 + B_{24}I)\rho_{44}(0) - \dot{\rho}_{44}(0). \tag{45}$$

Initial population densities required for the coefficients in Eqs. (31)–(33) are determined by steady-state values acquired prior to $t=0$ as determined in Sec. II A, for a specified intensity level. Initial time derivatives are calculated by substituting these initial populations directly into Eqs. (25)–(27).

The equations of motion can now be written in a convenient matrix form:

$$\dot{\rho} = A\rho + \mathbf{c}. \tag{46}$$

Here

$$\rho = \begin{pmatrix} \rho_{22} \\ \rho_{33} \\ \rho_{44} \end{pmatrix}, \quad A = \begin{pmatrix} a_{22} & a_{23} & a_{24} \\ a_{32} & a_{33} & a_{34} \\ a_{42} & a_{43} & a_{44} \end{pmatrix}, \quad \mathbf{c} = \begin{pmatrix} c_2 \\ c_3 \\ c_4 \end{pmatrix}.$$

Applying the method of Laplace transforms, and representing the transform of ρ by $\mathbf{R}(s)$, the equation of motion yields

$$s\mathbf{R}(s) - \rho(0) = A\mathbf{R}(s) + \frac{1}{s}\,\mathbf{c}. \tag{47}$$

The Laplace transform of the solution is therefore

$$\mathbf{R}(s) = (S-A)^{-1}\left[\rho(0) + \frac{1}{s}\,\mathbf{c}\right], \tag{48}$$

where S is s times the unit matrix and $\rho(0)$ is the initial value of ρ.

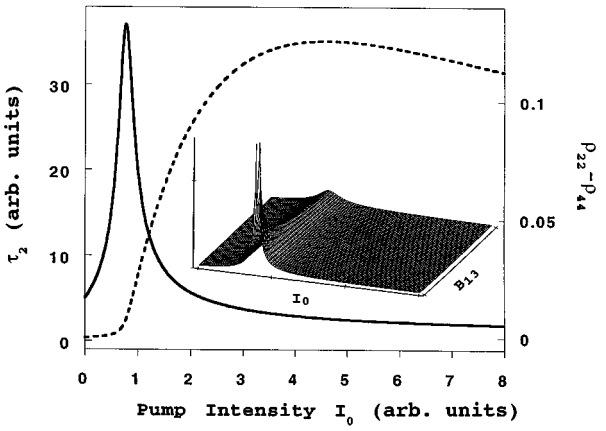

FIG. 3. The effective relaxation time of state $|2\rangle$ versus input intensity. The population difference $(\rho_{22}-\rho_{44})$ is graphed for direct comparison of the peak in the time constant with the threshold of avalanche absorption. Inset: Divergence of the response time τ_2 as the ground-state absorption rate B_{13} approaches zero, calculated numerically.

$\mathbf{R}(s)$ may be assumed to consist of a transient part and a steady-state part. That is, $\mathbf{R}(s)=\mathbf{R}^{\rm tr}(s)+\mathbf{R}^{\rm ss}(s)$. The steady-state part is readily identified as $\mathbf{R}^{\rm ss}(s)=-(1/s)A^{-1}\mathbf{c}$ since $\rho(\infty)=\lim_{s\to 0}[s\mathbf{R}(s)]=-A^{-1}\mathbf{c}$. The remainder of the solution transform must be the transient response. Consequently, the ith element of this transient part of the vector $R^{\rm tr}(s)$ is

$$R_i^{\rm tr}(s)=\frac{m_i s^2+n_i s+l_i}{s^3+Ms^2+Ns+L}, \tag{49}$$

where m_i, n_i, I_i, M, N, and L are all functions of elements of A, defined in the Appendix.

In the long-time limit $(s\to 0)$, $R^{\rm tr}(s)$ can be analyzed by partial fractions, or by the expansion of Eq. (49) to first order in s. Comparing the result

$$R_i^{\rm tr}(s)=\frac{1}{L/l_i(N/L-n_i/l_i)}\,\frac{1}{s+\dfrac{1}{N/L-n_i/l_i}} \tag{50}$$

with the general form of a transformed exponential, namely $\mathcal{L}\{ce^{at}\}(s)=c(s-a)^{-1}$, where c and a are constants, we find an effective time constant of

$$\tau_i=\frac{N}{L}-\frac{n_i}{l_i} \tag{51}$$

for level i. Calculations of the effective time constant τ_2 (for level 2) versus intensity in Fig. 3 reveal a dramatic ''slowing down'' at the avalanche threshold. The inset of Fig. 3 shows that τ_2 in fact diverges at a critical intensity as the ground-state absorption rate B_{13} approaches zero. This is a key result of the present research.

C. Wavelength dependence

A significant limitation of conventional analyses of the avalanche effect is that off-resonant excitation from the ground state which provides the seed population in the absorptive excited state is ignored. This omission is justified when steady-state populations are the only quantities of interest, for they depend negligibly on initial conditions (such as excited-state occupation). However to understand the wavelength dependence of the nonlinear refractive indices, the nonlinear dispersion, it is necessary to account for the initial (ground-state) absorption step in the avalanche process because of a surprising enhancement of the off-resonant ground-state polarization by the large excited-state populations generated through avalanche cross relaxation.

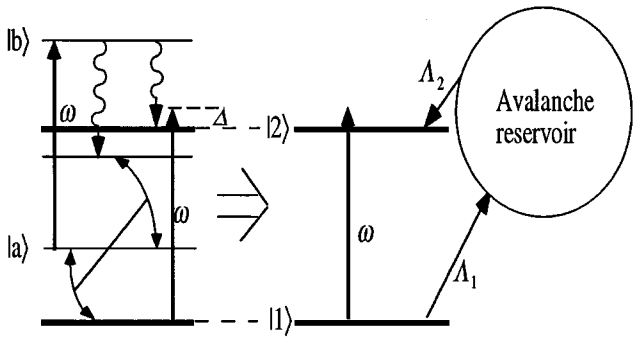

FIG. 4. A simplified model for the description of complex nonlinear susceptibility in avalanche systems. On the left is a multilevel sketch reflecting details of avalanche dynamics. On the right is a quasi-two-level model which retains aspects essential for understanding the nonlinear dispersion of avalanche nonlinearities.

In this section, the important role of the off-resonant absorption from the ground state which initiates the avalanche in determining polarization properties of the system is examined. Rather than calculating populations and polarizations from a five-level model which incorporates two optical transitions explicitly, it is very helpful to solve for the nonlinear dispersion in an equivalent two-step fashion using a quasi-three-level model which renders the basic physics much more obvious. To highlight the unexpectedly important role of the ground-state transition in determining nonlinear dispersion, we reduce the basic avalanche model to that shown on the right side of Fig. 4, in which all excited states but one are replaced by an incoherently pumped reservoir. The incoherent pumping rate Λ_1 is due exclusively to the nonradiative process of cross relaxation, whereas Λ_2 contains contributions from both cross relaxation and natural decay between levels. Both are functions of intensity. We show that detuning from the ground-state transition determines whether the nonlinear response is absorptive or dispersive.

After simplifying Eqs. (2)–(7) to reflect the model in Fig. 4, the equations of motion yield

$$\dot{\rho}_{11}=\gamma_{21}\rho_{22}-\Omega v-\Lambda_1=0, \tag{52}$$

$$\dot{\rho}_{22}=-\gamma_{21}\rho_{22}+\Omega v+\Lambda_2=0, \tag{53}$$

$$\dot{\tilde{\rho}}_{21}=-(\Gamma_{21}-i\Delta)\tilde{\rho}_{21}+\tfrac{1}{2}i\Omega(\rho_{22}-\rho_{11})=0. \tag{54}$$

$\Delta=\omega-\omega_{21}$ is the detuning of incident light at frequency ω from the transition frequency ω_{21} between levels. The closure relation $\rho_{11}+\rho_{22}+\rho_r=1$ accounts for the population density ρ_r circulating in the avalanche reservoir. The reservoir population ρ_r can serve as a free parameter or may be

determined explicitly from a multilevel model which takes the second photon interaction and cross relaxation into account. That is

$$\rho_r=\sum_i \rho_{ii},$$

where i runs over the indices of levels other than $|1\rangle$ and $|2\rangle$ in the full, microscopic model.

Using R to denote the rate per atom of decay to level $|2\rangle$ from the reservoir, we can apply the steady-state relation $\Lambda_1=\Lambda_2=R\rho_r$ to solve Eqs. (52)–(54) for ρ_{11}, ρ_{22}, and ρ_{21}:

$$\rho_{11}=\frac{\Delta^2+\Gamma_{21}^2+1/2|\Omega|^2\Gamma_{21}/\gamma_{21}}{\Delta^2+\Gamma_{21}^2+|\Omega|^2\Gamma_{21}/\gamma_{21}} - \frac{(1+R/\gamma_{21})(\Delta^2+\Gamma_{21}^2)+1/2|\Omega|^2\Gamma_{21}/\gamma_{21}}{\Delta^2+\Gamma_{21}^2+|\Omega|^2\Gamma_{21}/\gamma_{21}}\rho_r, \quad (55)$$

$$\rho_{22}=\frac{1/2|\Omega|^2\Gamma_{21}/\gamma_{21}}{\Delta^2+\Gamma_{21}^2+|\Omega|^2\Gamma_{21}/\gamma_{21}} + \frac{(\Delta^2+\Gamma_{21}^2)R/\gamma_{21}-1/2|\Omega|^2\Gamma_{21}/\gamma_{21}}{\Delta^2+\Gamma_{21}^2+|\Omega|^2\Gamma_{21}/\gamma_{21}}\rho_r, \quad (56)$$

$$\tilde{\rho}_{21}=\frac{(1/2)\Omega(\Delta-i\Gamma_{21})}{\Delta^2+\Gamma_{21}^2+|\Omega|^2\Gamma_{21}/\gamma_{21}}-\frac{(1/2)Q(\Delta-i\Gamma_{21})}{\Delta^2+\Gamma_{21}^2+|\Omega|^2\Gamma_{21}/\gamma_{21}} \times\left(1+\frac{2R}{\gamma_{21}}\right)\rho_r. \quad (57)$$

The effective susceptibility may be determined from $\tilde{P}(\omega)=\varepsilon_0\chi_{\rm eff}(\omega)\tilde{E}$. By decomposing the expression for $\chi_{\rm eff}(\omega)$ into linear and nonlinear parts using $\chi_{\rm eff}(\omega)=\chi^{(1)}(\omega)+\chi^{(3)}_{\rm eff}(\omega)|\tilde{E}|^2$, where the linear portion is given by the usual expression

$$\chi^{(1)}(\omega)=-\frac{N|\mu_{12}|^2\hbar^{-1}\varepsilon_0^{-1}(\Delta-i\Gamma_{21})}{\Delta^2+\Gamma_{21}^2},$$

the effective nonlinear susceptibility is found to be

$$\chi^{(3)}_{\rm eff}(\omega)=\left[\frac{4N|\mu_{12}|^4\hbar^{-3}\varepsilon_0^{-1}(\Delta-i\Gamma_{21})\Gamma_{21}/\gamma_{21}}{(\Delta^2+\Gamma_{21}^2)(\Delta^2+\Gamma_{21}^2+|\Omega|^2\Gamma_{21}/\gamma_{21})} + \frac{4N|\mu_{12}|^4\hbar^{-3}\varepsilon_0^{-1}(\Delta-i\Gamma_{21})(1+2R/\gamma_{21})}{\Delta^2+\Gamma_{21}^2+|\Omega|^2\Gamma_{21}/\gamma_{21}} \times(\rho_r/|\Omega|^2)\right]. \quad (58)$$

Notice that this result is quite different from the effective susceptibility in Eq. (24), which overlooked the ground-state transition. At the avalanche resonance, the excited-state detuning Δ' is zero. This means $\Delta'=\omega-\omega_{ba}=\Delta-(\omega_{ba}-\omega_{21})=0$, with the result that $\Delta=\omega_{ba}-\omega_{21}$. Under these conditions, the reservoir population is maximized and the real component of the nonlinear susceptibility is large *on resonance*. In fact, whenever $\Delta=\omega_{ba}-\omega_{21}>\Gamma_{21}$, the real part exceeds the imaginary part exactly on resonance.

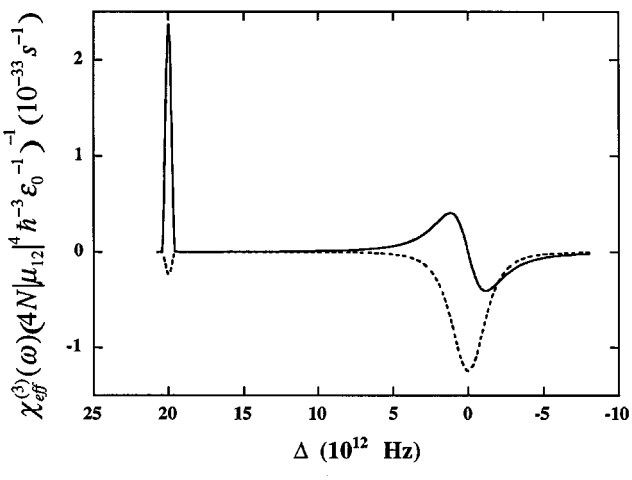

FIG. 5. Calculation of the real and imaginary components of an avalanche-induced nonlinear susceptibility. Parameters used in the calculation were $\Gamma_{21}=2\times10^{12}$ s^{-1} and $\gamma_{21}=2\times10^{8}$ s^{-1} (roughly appropriate for the $^3H_6\rightarrow{}^3F_3$ transition), and $\omega_{ba}-\omega_{21}=2\times10^{13}$ s^{-1}, $|\Omega|^2=3\times10^{18}$.

A direct comparison of the predicted behavior of nonlinear susceptibility components at a ground-state resonance ($\Delta=0$) and at an avalanche transition ($\Delta'=0$) is made in Fig. 5. For this plot, the reservoir population ρ_r was taken to have the steady-state value determined from the five-level model in the left side of Fig. 4. Notice that the real component passes through zero for $\Delta=0$ (ground-state transition) whereas it exhibits a maximum for $\Delta'=0$ (excited-state resonance). This is a second key result of the present research.

III. EXPERIMENT AND RESULTS

Avalanche upconversion can readily be observed in 1.5% Tm:$LiYF_4$ crystals at room temperature using dye laser excitation at 648 nm.[10] In this work we measured the nonlinear indices and characteristic response time of the avalanche nonlinearity in this material by a two-beam coupling technique. Details of the experimental method, analysis, and values of the induced indices have been described elsewhere.[11] Here we report on the temporal response and nonlinear dispersion over a wide wavelength range. Both these aspects of avalanche dynamics show unique features which provide an important basis for comparison with theory.

Figure 6 is a plot of the experimental response time measured in 1.5% Tm:$LiYF_4$ as a function of incident intensity. The avalanche threshold occurs at 1 W/cm^2. The important thing to notice is that both above and below the threshold intensity, the medium response is considerably faster than it is at the critical point. This indicates a dramatic slowing down of the effective lifetime of the absorptive excited state, right at the avalanche threshold.

By performing ultrahigh resolution scans of the beam-coupling spectrum at many different wavelengths in the red spectral region, additional results shown in Figs. 7 and 8 were obtained. The traces shown in Fig. 7 cover the region from the ground-state resonance near 688 nm to the excited-state resonance near 648 nm. It is immediately evident from the trend in their shapes, that the refractive index changes

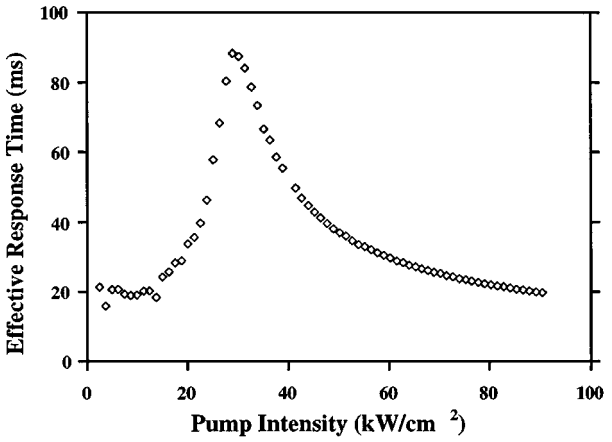

FIG. 6. Experimental response time of the avalanche medium versus intensity, obtained by two-beam coupling.

induced by incident light vary from primarily absorptive at 688 nm to primarily dispersive at 648 nm.

Quantitative analysis of the real and imaginary components[11] of these and other two-beam coupling spectra in the range 640–700 nm yielded the results shown in Fig. 8. In this figure it is somewhat easier to see that the real index goes through zero at the ground-state absorption resonance near 688 nm. By contrast, when the wavelength is tuned to the avalanche transition at 648 nm, the real index acquires a large value, exceeding the imaginary index by a factor of 2.

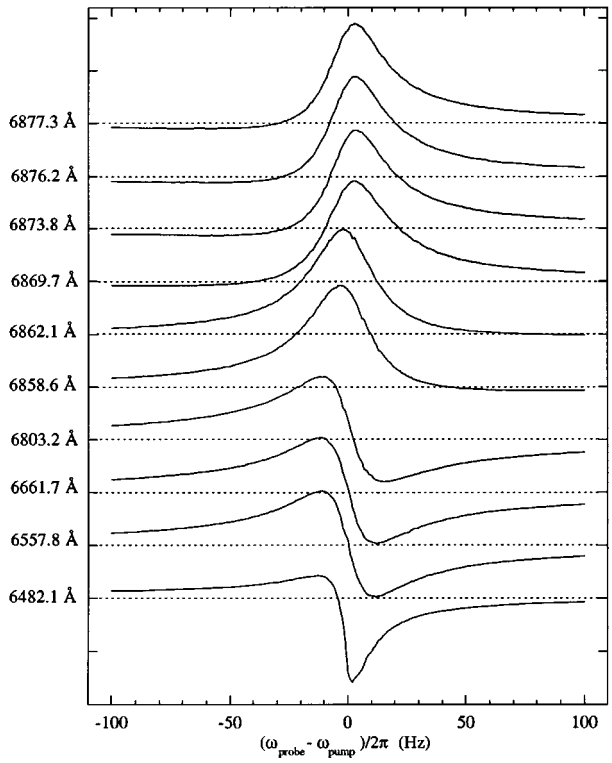

FIG. 7. Beam coupling spectra at different wavelengths between the ground-state absorption at 688 nm and the avalanche resonance at 648 nm.

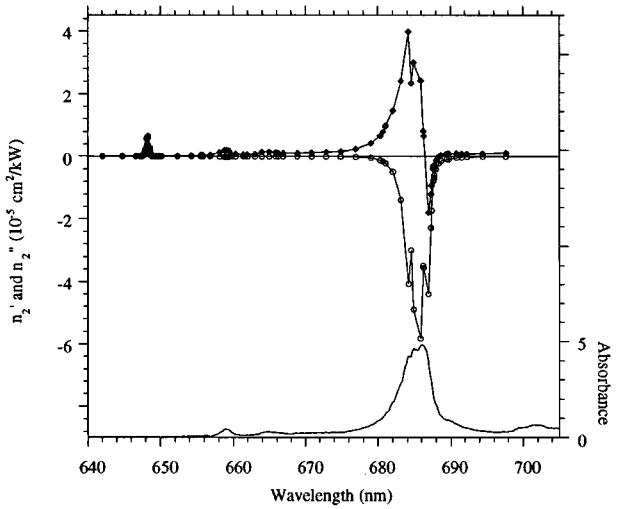

FIG. 8. Decomposition of the nonlinear susceptibilities determined by two beam coupling into real (diamonds) and imaginary parts (open circles). The spectral range includes an avalanche resonance at 648 nm and ground-state absorption at 688 nm. The lower trace gives the polarized absorption spectrum ($E\|C$) taken at room temperature which was used to correct the two-beam coupling signal in obtaining the nonlinear indices.

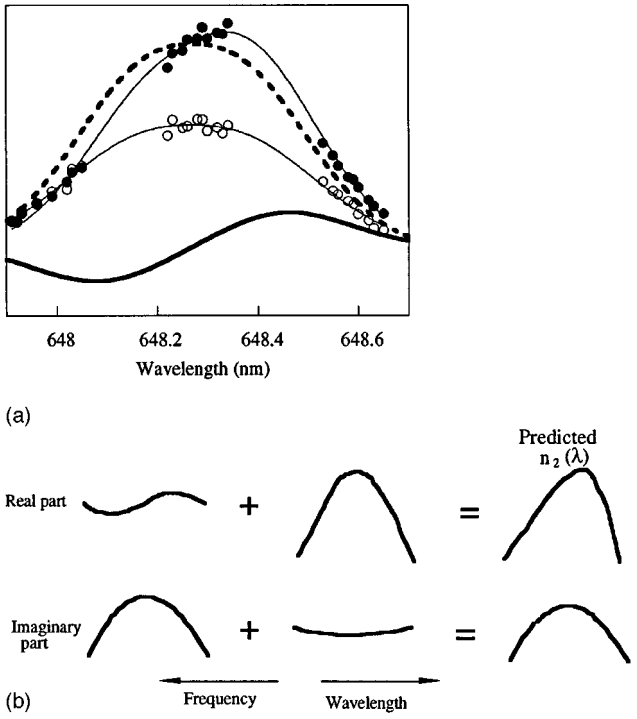

FIG. 9. (a) Decomposition of the real nonlinear index (filled circles) into symmetric and antisymmetric parts. The imaginary index is also shown (open circles), but is well described by a single Gaussian. Note the small relative shift between the experimental peaks of the two indices. (b) Schematic diagram showing the qualitative result of combining the nonlinear response associated with both optical transitions giving rise to avalanche absorption.

IV. DISCUSSION

The significant increase that is observed in optical response time at avalanche threshold typifies behavior of systems undergoing magnetic[12] or structural[13] phase transitions. It is well known, for example, that the characteristic time of spin correlations in interacting spin systems undergoes critical slowing down[14] at order-disorder transitions. The phase transition in our system consists of the sudden appearance of an excited-state population above a critical intensity and occurs at the threshold intensity determined by Eq. (20). The temporal response time does indeed diverge ($\tau\rightarrow\infty$) as the ground-state absorption rate approaches zero. Hence we refer to this as critical slowing down. A spin analogy may be particularly apt, since optical cross relaxation, in which a first atom undergoes nonradiative deexcitation while a second, coupled atom conserves energy by making a dipole transition to an excited state, is formally equivalent to secular spin-spin interactions. The critical role of temperature in a spin-ordering transition is replaced here by a critical dependence on optical intensity. Certainly it would be interesting to explore adaptations of the continuous-spin Ising model to avalanche dynamics. Also, additional experiments of the type we have reported here should be very fruitful for more detailed studies of avalanche critical exponents and phenomena.

Figure 9(a) shows the result of a decomposition of the measured indices into polarization contributions arising from the two optical transitions in the problem. Figure 9(b) shows schematically how the two contributions add to give a slightly asymmetric real component and an imaginary component which is diminished by an excited-state contribution of opposite sign. Notice that the decomposition accounts satisfactorily for the slight asymmetry observed in the real index peak. The real index peak is shifted with respect to the imaginary index curve due to a small dispersively shaped contribution from the resonant excited-state transition.

These findings are in excellent agreement with the quasi-two-level theory of Sec. II C. Because details of the cross-relaxation dynamics are omitted in this model of nonlinear dispersion, it can be concluded that the predominantly real nonlinear susceptibility encountered in our experiments at the excited-state absorption resonance is not limited to avalanche systems. Rather, it is a property of all systems in which excitation greatly detuned from any ground-state transition nevertheless generates large excited-state populations. Avalanche systems provide merely one example where this occurs, with the cross-relaxation dynamics constituting the mechanism whereby excited states develop large populations nonradiatively.

ACKNOWLEDGMENT

This research was sponsored in part by the Air Force Office of Scientific Research (H. Schlossberg).

APPENDIX

Explicit expressions for the quantities in Eq. (49) are

$$m_2=x^{-1}[-a_{33}a_{44}c_2+a_{23}a_{44}c_3+(a_{24}a_{33}-a_{23}a_{34})c_4]+\rho_{22}(0), \tag{A1}$$

$$m_3=x^{-1}[(a_{32}a_{44}-a_{42}a_{34})c_2+(a_{42}a_{24}-a_{22}a_{44})c_3+(a_{34}a_{22}-a_{24}a_{32})c_4]+\rho_{33}(0), \tag{A2}$$

$$m_4=x^{-1}[a_{42}a_{33}c_2-a_{23}a_{42}c_3+(a_{32}a_{23}-a_{22}a_{33})c_4]+\rho_{44}(0), \tag{A3}$$

$$\begin{aligned} n_2=x^{-1}[&(a_{33}^2a_{44}+a_{33}a_{44}^2+a_{32}a_{23}a_{44}-a_{42}a_{23}a_{34}+a_{42}a_{24}a_{33})c_2-a_{23}a_{44}(a_{22}+a_{33}+a_{44})c_3\\ &+(a_{23}a_{34}-a_{24}a_{33})(a_{22}+a_{33}+a_{44})c_4-(a_{33}+a_{44})x\rho_{22}(0)]+a_{23}\rho_{33}(0)+a_{24}\rho_{44}(0), \end{aligned} \tag{A4}$$

$$\begin{aligned} n_3=x^{-1}[&(a_{42}a_{34}-a_{32}a_{44})(a_{22}+a_{33}+a_{44})c_2+(a_{32}a_{23}a_{44}-a_{42}a_{23}a_{34}-a_{24}a_{42}a_{22}-a_{44}a_{42}a_{24}+a_{22}^2a_{44}+a_{44}^2a_{22})c_3\\ &+(a_{24}a_{32}-a_{34}a_{22})(a_{22}+a_{33}+a_{44})c_4]+a_{32}\rho_{22}(0)-(a_{22}+a_{44})\rho_{33}(0)+a_{34}\rho_{44}(0), \end{aligned} \tag{A5}$$

$$\begin{aligned} n_4=x^{-1}[&-a_{42}a_{33}(a_{22}+a_{33}+a_{44})c_2+a_{23}a_{42}(a_{22}+a_{33}+a_{44})c_3+(a_{22}^2a_{33}+a_{42}a_{24}a_{33}+a_{22}a_{33}^2-a_{32}a_{23}a_{22}-a_{33}a_{32}a_{23}\\ &-a_{42}a_{23}a_{34})c_4]+a_{42}\rho_{22}(0)-(a_{22}+a_{33})\rho_{44}(0), \end{aligned} \tag{A6}$$

$$\begin{aligned} l_2=x^{-1}[&(-a_{33}^2a_{44}^2+a_{44}a_{42}a_{23}a_{34}+a_{33}a_{42}a_{23}a_{34}-a_{33}^2a_{42}a_{24}-a_{44}^2a_{32}a_{23})c_2+a_{23}(-a_{42}a_{23}a_{34}-a_{44}a_{42}a_{24}+a_{42}a_{24}a_{33}+a_{44}^2a_{22}\\ &+a_{33}a_{44}^2)c_3+(a_{24}a_{33}^2a_{22}+a_{23}^2a_{34}a_{32}+a_{24}a_{32}a_{23}a_{44}-a_{23}a_{34}a_{22}a_{33}-a_{23}a_{34}a_{22}a_{44}-a_{23}a_{34}a_{33}a_{44}+a_{24}a_{33}^2a_{44}\\ &-a_{24}a_{33}a_{32}a_{23})c_4]+a_{33}a_{44}\rho_{22}(0)-a_{23}a_{44}\rho_{33}(0)+(a_{23}a_{34}-a_{24}a_{33})\rho_{44}(0), \end{aligned} \tag{A7}$$

$$l_3 = x^{-1}[(a_{32}a_{44}^2a_{22} + a_{32}a_{44}^2a_{33} - a_{32}a_{44}a_{42}a_{24} + a_{32}a_{42}a_{24}a_{33} - a_{34}a_{42}a_{22}a_{33} - a_{34}a_{42}a_{22}a_{44} - a_{34}a_{42}a_{33}a_{44} + a_{34}a_{42}^2a_{24})c_2$$
$$+ (-a_{24}a_{42}a_{32}a_{23} - a_{24}^2a_{42}^2 - a_{22}^2a_{44}^2 + a_{22}a_{42}a_{23}a_{34} - a_{44}^2a_{32}a_{23} + a_{44}a_{42}a_{23}a_{34} + 2a_{24}a_{42}a_{22}a_{44})c_3 + (a_{34}a_{32}a_{23}a_{44}$$
$$- a_{34}^2a_{42}a_{23} + a_{34}a_{42}a_{24}a_{33} + a_{34}a_{22}^2a_{33} + a_{34}a_{22}^2a_{44} - a_{34}a_{22}a_{32}a_{23} - a_{34}a_{22}a_{42}a_{24} - a_{24}a_{32}a_{22}a_{33} - a_{24}a_{32}a_{22}a_{44}$$
$$- a_{24}a_{33}a_{32}a_{44} + a_{24}a_{32}^2a_{23} + a_{24}^2a_{32}a_{42})c_4] + (a_{42}a_{34} - a_{32}a_{44})\rho_{22}(0) + (a_{22}a_{44} - a_{42}a_{24})\rho_{33}(0) + (a_{24}a_{32} - a_{34}a_{22})\rho_{44}(0), \tag{A8}$$

$$l_4 = x^{-1}[a_{42}(-a_{42}a_{23}a_{34} - a_{33}a_{32}a_{23} + a_{22}a_{33}^2 + a_{33}^2a_{44} + a_{32}a_{23}a_{44})c_2 - a_{42}a_{23}(a_{22}a_{33} - a_{32}a_{23} + a_{22}a_{44} + a_{33}a_{44} - a_{42}a_{24})c_3$$
$$+ (-a_{33}^2a_{42}a_{24} + a_{22}a_{42}a_{23}a_{34} + a_{33}a_{42}a_{23}a_{34} - a_{24}a_{42}a_{32}a_{23} - a_{22}^2a_{33}^2 + 2a_{22}a_{33}a_{32}a_{23} - a_{32}^2a_{23}^2)c_4] - a_{42}a_{33}\rho_{22}(0)$$
$$+ a_{42}a_{23}\rho_{33}(0) + (a_{22}a_{33} - a_{32}a_{23})\rho_{44}(0), \tag{A9}$$

$$M = -(a_{22} + a_{33} + a_{44}), \tag{A10}$$

$$N = a_{22}a_{33} - a_{32}a_{23} + a_{22}a_{44} + a_{33}a_{44} - a_{24}a_{42}, \tag{A11}$$

$$L = x, \tag{A12}$$

where

$$x = a_{32}a_{23}a_{44} + a_{42}a_{24}a_{33} - a_{42}a_{23}a_{34} - a_{22}a_{33}a_{44}.$$

[1] J. Chivian, W. Case, and D. Eden, Appl. Phys. Lett. **35**, 124 (1979).

[2] M. E. Koch, A. W. Kueny, and W. E. Case, Appl. Phys. Lett. **56**, 1083 (1990); T. Hebert, R. Wannemacher, R. M. Macfarlane, and W. Lenth, *ibid*. **60**, 2592 (1992).

[3] A. Kueny, W. E. Case, and M. E. Koch, J. Opt. Soc. Am. B **6**, 639 (1989).

[4] Q. Shu, Ph.D. thesis, University of Michigan, 1996.

[5] Q. Shu, H. Ni, and S. C. Rand, Opt. Lett. **22**, 123 (1997).

[6] A preliminary report of these findings was given by Q. Shu and S. C. Rand, in *Proceedings of the Conference on Lasers and Electro-optics, Anaheim, California, 1996 (CLEO/QELS' 1996)* (Optical Society of America, Washington D.C., 1996).

[7] See, for example, S. Stenholm, *Foundations of Laser Spectroscopy* (Wiley, New York, 1984).

[8] M. F. Joubert, S. Guy, and B. Jacquier, Phys. Rev. B **48**, 10 031 (1993).

[9] P. Xie and S. Rand, J. Opt. Soc. Am. B **11**, 901 (1994).

[10] H. Ni and S. C. Rand, Opt. Lett. **16**, 1424 (1991).

[11] D. Redman, Q. Shu, A. Lenef, and S. C. Rand, Opt. Lett. **17**, 175 (1992).

[12] M. E. Fisher, Rev. Mod. Phys. **46**, 597 (1974).

[13] J. F. Scott, Rev. Mod. Phys. **46**, 83 (1974).

[14] For an excellent introduction to analogies in critical phenomena, see H. Haken, Rev. Mod. Phys. **47**, 67 (1975).